Properties of an electron source with laser-induced electron emission

G. Siller, E. Buchelt, H.B. Schilling

IPP 0/7 April 1971

MAX-PLANCK-INSTITUT FÜR PLASMAPHYSIK

GARCHING BEI MÜNCHEN

MAX-PLANCK-INSTITUT FÜR PLASMAPHYSIK

GARCHING BEI MÜNCHEN

Properties of an electron source with laser-induced electron emission

G. Siller, E. Buchelt, H.B. Schilling

IPP 0/7 April 1971

Die nachstehende Arbeit wurde im Rahmen des Vertrages zwischen dem Max-Planck-Institut für Plasmaphysik und der Europäischen Atomgemeinschaft über die Zusammenarbeit auf dem Gebiete der Plasmaphysik durchgeführt.

IPP 0/7

G. Siller
E. Buchelt
H.B. Schilling

Properties of an electron source with laser-induced electron emission (April 1971) - in English

Abstract

In this report, measurements of the emittance of a pulsed electron source with laser-induced electron emission are described. The energy spread of the electrons in the pulse is evaluated by deflection in a static magnetic field. This source is to be used in an electron ring accelerator.

INTRODUCTION

This report is a continuation of the report entitled "Laser-induced emission of strong electron pulses in the nanosecond range" by G. Siller, K. Büchl, E. Buchelt (IPP 0/2, IPP 3/100), which was published in June 1969. In both cases the experimental results with a new type of electron source - to be used in an electron ring accelerator - are described. The problem was to develop a source which can deliver electron pulses with an amplitude of several hundred amperes and a length of the order of 10^{-8} seconds. One of the main requirements of the electron ring accelerator in this electron source was to have this current in a small emittance. One way to keep the emittance low is to make the electron source as punctiform as possible. The idea was now to focus the beam of a pulsed high-power laser on a metal plate to draw out electrons. The focal spot of a laser beam has, in practice, an area of 10^{-2} to 10^{-4} cm^2. If it is possible in this way to produce an electron current pulse of the required magnitude and pulse length, this electron source should be very suitable for the electron ring accelerator.

In the above-mentioned report we described the experimental setup we used to produce the electron current pulses and to separate them from the metal plasma cloud, which is also drawn out by focussing the laser beam on a metal target surface. The main results are repeated in the next section. In this report we give an account of the measurements of the emittance. Another most important quantity for the electron ring accelerator is the energy spread of the electrons in the pulse. This spread is measured in a static magnetic field and the results are also described.

Production of electron pulses

In this section we shall briefly repeat the results described in the above-mentioned report in order to give a complete picture of the electron source to those readers, to whom the first report is not available. In the first experimental setup used, all the main effects that occur when a laser beam hits a metal surface can be studied. This arrangement can be seen in Fig. 1a. The cathode of our circuit was a tantalum plate on which we focussed a ruby laser beam. The output energy was 0.1 joule and the half-width of the laser pulse was 17 nsec (about 6 MW). The anode was grounded by a 0.5Ω coaxial resistor. The voltage drop across this resistor was measured with a Tektronix 519. The voltage source was a low-inductance capacitor of 60 nF. The capacitor was charged to -1KV. The cathode-to-anode distance was 4 cm.

The measured current pulse can be seen in Fig. 1b. The main part of the pulse consists of a damped oscillation in front of which a small negative pulse can be seen. The laser pulse coincides with the beginning of this small negative pulse. For the oscillogram we have the following explanation: The first small negative pulse is produced by electrons emitted by the cathode when the laser beam hits the surface of the tantalum target. After a certain time delay an expanding tantalum plasma reaches the anode and produces a short circuit between the cathode and anode. The capacitor is discharged across this plasma cloud by a damped oscillation. The measured oscillation frequency agrees well with the estimated data in the circuit. If one computes the velocity with which the plasma expands away from the target surface according to Fig. 1 b, one gets velocities up to 10^7 cm/sec. These results showed a limitation in the application of this electron source: The electron pulse length is terminated by the time of flight of the plasma cloud between the cathode and anode.

In order to separate now the electron pulse from the plasma cloud, the capacitor was replaced by another circuit which allows the voltage between cathode and anode to be switched off before the expanding plasma from the target has reached the anode. This improved experimental setup can be seen in Fig. 2. The capacitor of Fig. 1a is now replaced by a coaxial line with a characteristic impedance Z of, for example, 30 Ω. This line was terminated at one end by a series connection of an ohmic load R equal to Z and a laser triggered spark gap. The other end of the line was connected to the cathode and anode of the circuit. With this arrangement the voltage at the cathode can be switched off after a time given by the delay time of the coaxial line. We used this voltage source in the range of -30 to -60 KV. The ultimate pressure in the vacuum chamber was about 10^{-6} torr. We used a two-stage Q-switched ruby laser with an energy up to 8 joule and a half-width of the laser pulse of 17 nsec. The beam divergence was 5 mrad. With the focal length of the focussing lens between 5 and 15 cm the focal spot has a radius of 2.5 to 7.5×10^{-2} cm . Therefore, the power density was of the order of 10^{10} W/cm^2.

Characteristic current pulses obtained with this experimental setup are shown in Fig. 3 and 4. In both cases the charging voltage of the line was -30 KV. In Fig. 3 the line length was 5.5 m and in Fig. 4 it was 16 m. This results in two electron pulses with different lengths. With the maximum energy available and extremely good focussing we achieved pulses with amplitudes of up to 1000 amperes. In an additional experiment we identified the charge carriers in these negative pulses to be really free electrons by deflecting them in a static electric field.

Emittance measurements

The most interesting quantity of the electron source is the current that can be obtained in a certain emittance. The experimental setup with which this was measured can be seen in Fig. 5. The tantalum plate of the cathode was surrounded by an electrode to shape the electric field lines (Pierce optical system). The anode was a grounded ring with an inner diameter of 1 cm. This ring was continued on one side by a cone so that only electrons passing through the ring can reach the emittance box. The cathode-to-ring distance was 4 cm. The cathode was charged to -60 KV. The voltage source was the coaxial storage line described in Fig. 2. The total current emitted by the cathode was measured by the upper beam toroid (Rogowski coil) and the current to the emittance box was measured by the lower one.

We determined the emittance in the central part of the electron beam. The emittance box consisted of a 1.5 mm thick metal plate with an array of apertures 0.3 mm in diameter. The array of the holes in the box is shown in Fig. 6. A film (Agfa Gevaert N 33) wrapped in 10 μ aluminium foil was mounted at a distance of 2 cm behind the plate. The range of 60 KV electrons in aluminium is 20 μ. A photograph of the irradiated film can be seen in Fig. 7. The distance of the holes in the emittance box must be so large that the density curves of the holes on the film do not overlap. The black sectors in Fig. 6 and 7 are for calibrating the density of the film. In this area there is a piece cut out of the metal plate of the emittance box and the electrons hit the wrapped film directly. The film is exposed to four electron pulses. In Fig. 7 the black sector is divided into four subsectors. The subsector 1 is hit by one electron pulse, the next by two, the next by three and the darkest one by four equal electron pulses. The difference

in the density of the four subsectors cannot be seen very well in this reproduction, but is clear on the exposed film. The photometric curves along these four subsectors in the radial direction are seen in Fig. 8. The sharp line at the radius zero is the density curve of the hole in the center of the emittance box. By measuring the photometric curves of the exposed film, the density anywhere is always compared with the density of the hole in the center of the emittance box. Therefore, if one draws in Fig. 8 a line parallel to the abscissa, touching the maximum of the center curve, this line cuts the photometric curve for intensity 1 (four electron pulses) at point A. E-A is the density for the intensity 1, E-B the density for the intensity 3/4 (three electron pulses), E-C is for intensity 1/2 (two electron pulses), and E-D for intensity 1/4 (one electron pulse). With these values in Fig. 9 a curve is drawn giving the density of the film versus the intensity. This curve is extrapolated to zero and therefore one gets also the density for the intensities 1/8 and 1/16.

For evaluating the emittance of the electron source a radial trace of five points in Fig. 7 was used. This trace is denoted by an arrow. The photometric curve, which gives the density curve of the five points versus the radius is plotted in Fig. 10. The light spot of the photometer is smaller than the diameter of the density points in Fig. 7. The first number in Fig. 10 at each peak gives the radius in millimeters where the adequate hole is situated on the metal plate of the emittance box. The second number, in parenthesis, gives the radius in millimeters where the density curve on the film has its maximum. These numbers agree with the values on the abscissa in Fig. 10. The scale on the ordinate for the intensities between 1 and 1/16 is taken from Fig. 9.

The area of the five curves shown in Fig. 10 must be measured. For this purpose the curves were plotted again, but with a

linear scale of the intensity. For greater accuracy the values of the abscissa were increased by a factor 10 and those of the ordinate increased so that the center curve fills one page. In this form the curves are not yet suitable to be measured. According to the finite angular acceptance of the apertures the ordinate of the curves must be multiplied by a factor K, which is 1 for the center curve and greater than 1 for the other curves. The factor K rises with increasing distance of the apertures from the center. Figure 11 shows the method of computing the factor K. Figure 11a gives a cross section of an aperture. The diameter of the hole is 0.3 mm and the effective thickness of the metal plate is 0.5 mm. The upper edge of the hole prevents electrons from coming through for -0.15 mm $>$ x $>$ +0.15 mm in the coordinate system given in Fig. 11 b. For the angle φ one gets $-\frac{\pi}{2} < \varphi < \frac{\pi}{2}$. The lower edge of the hole gives an additional limitation of the angle φ, depending on the position x. One gets $|\varphi_{max}| = \frac{0.3\,mm}{0.5\,mm} = 0.6\,rad$. The limitation curves for the upper and lower edge of the aperture are drawn in Fig. 11 b. The allowed region for the electrons to come through an aperture is given by the unhatched parallelogram in Fig. 11 b. For the center line in Fig. 10 the focal point of the laser from which the electrons are coming, the center hole in the emittance box, and the center of the exposed film (Fig. 7) are all on the axis of the experimental setup. For all electrons passing through the center hole the mean value $\langle\varphi\rangle$ of φ is zero and, therefore, the factor K is 1. For the apertures of the emittance box outside the axis $\langle\varphi\rangle \neq 0$. In this case (see Fig. 11 b) the number of electrons flying through this aperture is reduced by a factor AB/AC $<$ 1 by the finite angular acceptance. Therefore, the ordinate of the corresponding density curve must be multiplied by $K = \frac{AC}{AB} > 1$. This was done with the curves in Fig. 10. The result can be seen in Fig. 12. The values of $\langle\varphi\rangle$ were computed for each curve

from the radial shift between the position of the aperture in the metal plate and the maximum density of the respective curve on the film - given by the two numbers at each peak in Fig.10 - and the distance between metal plate and film.

Figure 13 provides a sketch defining all values that have been measured in the curves in Fig. 12. The table on page 8 gives the results. The angles α_1 and α_3 were measured for the intensities 1/2 and 1/4. The angle α_2 is identical with $\langle\varphi\rangle$. In Fig. 12 for all five curves the areas A_{total} of the total curve, $A_{1/4}$ for 1/4 of the intensity and $A_{1/2}$ for 1/2 of the intensity were measured as sketched in Fig. 12. The results are also given in the table on page 8. One gets for

$$\Sigma A_{total} = 357.4 \text{ cm}^2$$

$$\Sigma A_{1/4} = 258.6 \text{ cm}^2$$

$$\Sigma A_{1/2} = 191.9 \text{ cm}^2$$

For evaluating the emittance ϵ in Fig. 14 lines of constant density were drawn in a two-dimensional phase-space diagram. These two curves are for 1/2 and 1/4 of the maximum phase density. The area within the closed curves of 1/2 of the maximum phase density was 31.4 mrad.cm and 63.6 mrad.cm within the 1/4 curve. The 1/2 curve contained

$$\frac{\Sigma A_{1/2}}{\Sigma A_{total}} = 0.537$$

i.e. about 54 % of the current to the emittance box. For the 1/4 curve one gets

$$\frac{\Sigma A_{1/4}}{\Sigma A_{total}} = 0.723$$

Table of the measured values

a [mm]	b [mm]	α_1 [mrad]	α_3 [mrad]	α_1 [mrad]	α_3 [mrad]	α_2 [mrad]	K	A [cm^2] total	A [cm^2] 1/4	A [cm^2] 1/2
0	0	-11.3	+8.0	-16.0	+9.5	0	1.000	105.9	89.6	79.7
4.50	5.10	+22.3	+39.3	+18.8	+42.3	+30.0	1.052	99.5	82.9	72.7
8.00	9.15	+51.8	+64.5	+45.8	+70.0	+57.5	1.106	79.6	58.4	39.5
12.50	14.25	-	-	+78.5	+96.8	+87.5	1.171	52.6	27.7	-
16.50	19.05	-	-	-	-	+127.5	1.271	19.8	-	-

for 1/2 of the maximum intensity

for 1/4 of the maximum intensity

i.e. about 72 %. The total current emitted by the tantalum plate was of the order of several hundred amperes. The current within the area where the emittance was measured was I = 17 A. That means a current of I = 9.12 A in an emittance of ϵ = 31.4 mrad.cm or a current of I = 12.3 A in an emittance of ϵ =63.6 mrad.cm. With these values of the emittance and the current one can compute the normalized brightness. This quantity is given by the formula

$$B = \frac{I}{\epsilon^2 \cdot eU\,(1 + eU/2m_0c^2)}$$

where eU is the kinetic energy and m_0c^2 the rest energy of the electrons. With the evaluated values one gets

$$B_{1/2} \approx 1.5 \cdot 10^{-1} \left[\frac{A}{\text{sterad.cm}^2 \cdot \text{eV}}\right]$$

and

$$B_{1/4} \approx 4.8 \cdot 10^{-2} \left[\frac{A}{\text{sterad.cm}^2 \cdot \text{eV}}\right]$$

With our present field emission tube in the electron ring accelerator we got a brightness of the order of 10^{-3} A/sterad·cm^2·eV and with hot cathodes (Ardenne) one gets a few times 10^{-4} A/sterad·cm^2·eV.

It is our opinion that the values evaluated for the emittance are only an upper limit, and that the real values are smaller. Therefore, the values of the real brightness are larger than those computed above. There are two reasons for this assumption. The first reason can be seen in Fig. 12. The width of the photometric curves is of the same order as the diameter of 0.3 mm of the apertures. One would therefore expect that a smaller diameter of the apertures would also reduce the width of the photometric curves and the value of the emittance. Smaller apertures, however, have two disadvantages: Firstly, the intensity of the

electron current pulse is greatly reduced and the density of the film becomes insufficient. Secondly, it is difficult to drill such small holes.

The second reason for our assumption that the real emittance is smaller is as follows: We measured the emittance with a film, i.e. time-integrated over the pulse length. The voltage pulse is not a rectangle, and so electrons with different kinetic energies are recorded. This effect will also increase the emittance, although this influence is partially cancelled out by the aluminium foil in which the film was wrapped. When the kinetic energy of the electrons becomes too low these particles stick fast in the foil.

Experiments with higher accelerating voltages

For measuring the electron pulse an accelerating voltage of -30 KV was applied (see Fig. 2). The emittance was evaluated with the experimental setup shown in Fig. 5. The applied voltage was -60 KV. In both cases the voltage source was a storage line in conjunction with a laser-triggered spark gap as mentioned above. For accelerating voltages equal or greater than -100 KV we used a Blumlein cable with an impedance of 80Ω. The experimental arrangement for resonant pulse charging up to -200 KV with a Marx generator can be seen in Fig. 15. An alternative method of stationary charging up to -100 KV could be applied by means of a high voltage cascade generator. The cathode-anode system was the same as in Fig. 5, only the anode was now a grounded disk.

The cable was fired by an additional 100 MW laser. The current we obtained versus the voltage is plotted in Fig. 16. The maximum was 800 amperes for about 200 KV. The lower curve was

measured when the Blumlein pulse at the cathode-anode gap appeared at the same time as the laser pulse. Higher currents for the same voltage were reached when the laser was fired 20 nsec before the voltage pulse was applied. In this time the laser-produced metal plasma cloud at the cathode spreads out, and the area from which the electrons are extracted is larger.

Measurements of the energy spread

The next quantity in which we were interested was the energy spread of the electrons in the pulse. The energy of the electrons was measured by deflecting them in a static magnetic field. The chosen radius of curvature of the electrons in the magnetic field was about 10 cm. This corresponds to a field strength of about 110 gauss for 100 KeV electrons. The measuring device for the electrons was an arrangement of 14 collectors each in the form of a strip with a width of 1 mm, a height of 14 mm, and a distance of 1 mm from the next strip. A change of 1 % in the energy of the particles resulted in a deflection of about 1 mm at the place where the 14 collectors were mounted. For these measurements the voltage at the cathode was of the order of -100 KV. For a rectangular voltage pulse of the Blumlein generator one would expect an electron energy according to the applied voltage superimposed by the energy spread of the source. The results were discouraging because the voltage pulse deviated appreciably from a rectangle. Because of the rise and fall of the voltage the electron current swept rather fast across the detector. Each energy appeared twice and at each collector two current pulses were measured. This effect can be seen in Fig. 17 for two collectors 7 and 8. Collector 8 measured the electrons with the lower energy. With rising

voltage, first a pulse appeared at collector 8 and then at collector 7. When the voltage falls, first the pulse is measured at collector 7 and then at collector 8. When the strength of the static magnetic deflection field is enhanced, the distance between the two pulses is reduced. Although these results were not satisfying, it is a simple matter to evaluate an upper limit of the energy spread. In Fig. 18 an idealized voltage pulse can be seen with a gradient of 1 KV/nsec. If, for instance, one edge of a strip in the detector is hit by 100 KeV electrons, the other edge is hit by 101 KeV electrons. This results from the values mentioned above for the width of one strip and for the deflection of the beam caused by a change of 1 % in the particle energy. With no energy spread one would therefore expect a current pulse length Δt_1 at the strip according to the rising voltage. If ε is the energy spread of the source, this causes a longer pulse length Δt_2. One gets the relation (see Fig. 18)

$$A = \frac{1}{\Delta t_1}\left[\frac{KV}{nsec}\right] = \frac{\varepsilon + 1}{\Delta t_2}\left[\frac{KV}{nsec}\right]$$

With the values for A known from the voltage pulse and for Δt_2 measured from the current pulse length at a strip, one gets $\varepsilon \leq 800$ eV as an upper limit, i.e. the energy spread is smaller than 1 %. Values of about 100 eV for the electron temperature were also measured by other authors who produced a metal plasma by focussing a laser beam on a target. We hope that the value for ε is not increased by accelerating the particles to an energy of 2 MeV, which is the injection energy into the electron ring accelerator.

Further development

Comparing the results of the measurements with the requirements of the electron ring accelerator one could expect that this source should be suitable. We are therefore continuing with the development of the source. We now intend constructing a water-filled Blumlein cable with a transformation line which should give us an accelerating voltage of 2 MV. In the meantime we will test the laser electron source with the 2 MV voltage generator we use for our field emission tube. For this purpose we shall develop a source with electrostatic beam focussing. We also need a suitable laser in order to get higher repetition rates. With the power necessary in our case we are thinking of using a liquid laser.

The authors wish to thank Prof. A. Schlüter for suggesting this investigation and Dr. C. Andelfinger for his advice during the experiments. The authors are also grateful to a number of colleagues for clarifying discussions, especially to Dr. W.Ott for his assistance in evaluating the emittance and to Dr. W. Dommaschk for his numerical calculations concerning the magnetic spectrometer.

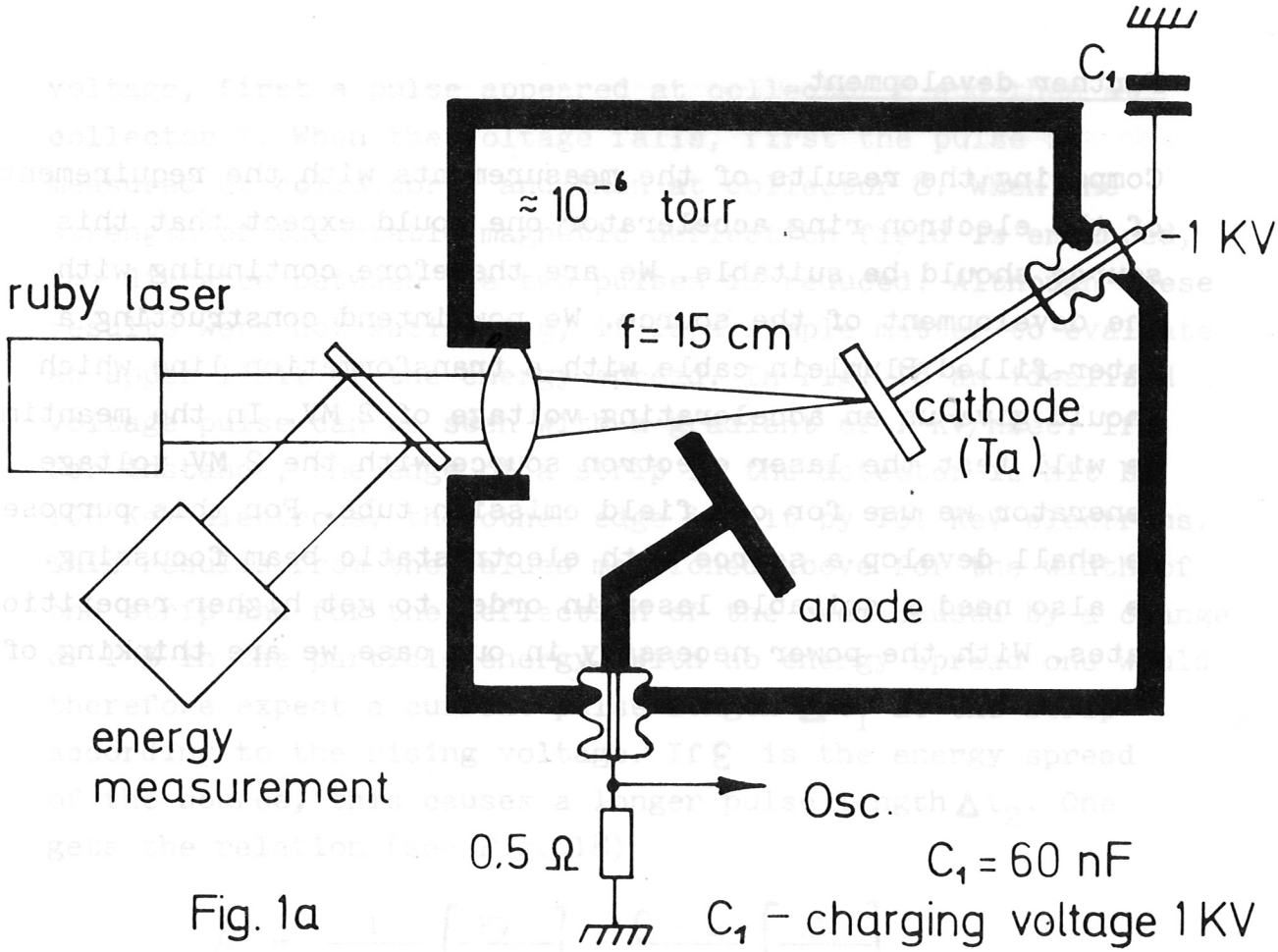

Fig. 1a

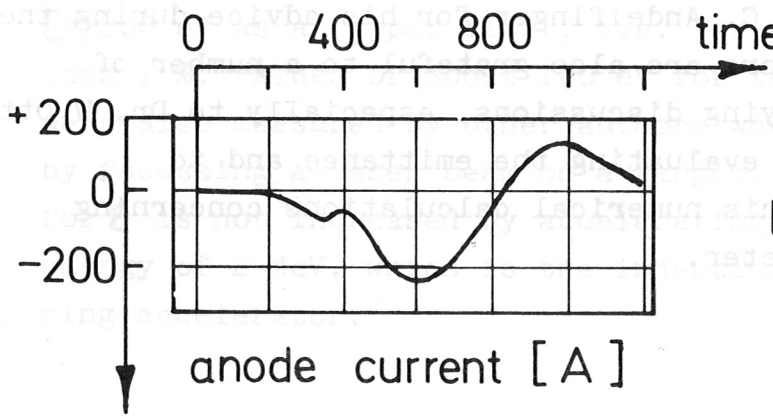

laser 0.1 joule

Fig. 1b

Fig. 1a) Experimental setup of the first experiment

1b) Current pulse

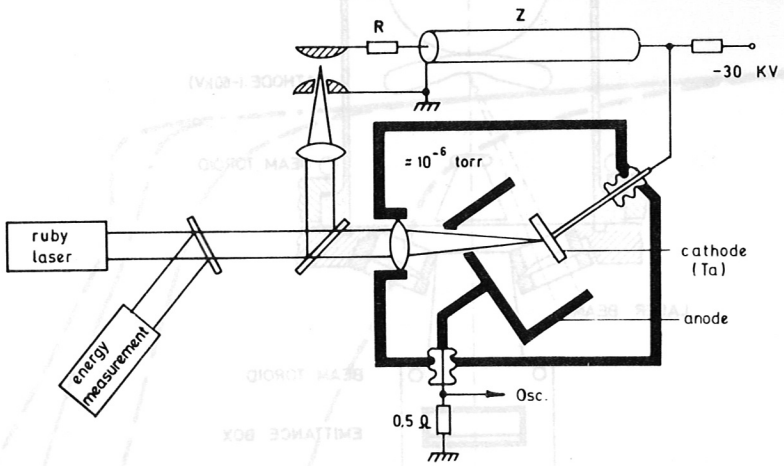

Fig 2. Improved experimental setup

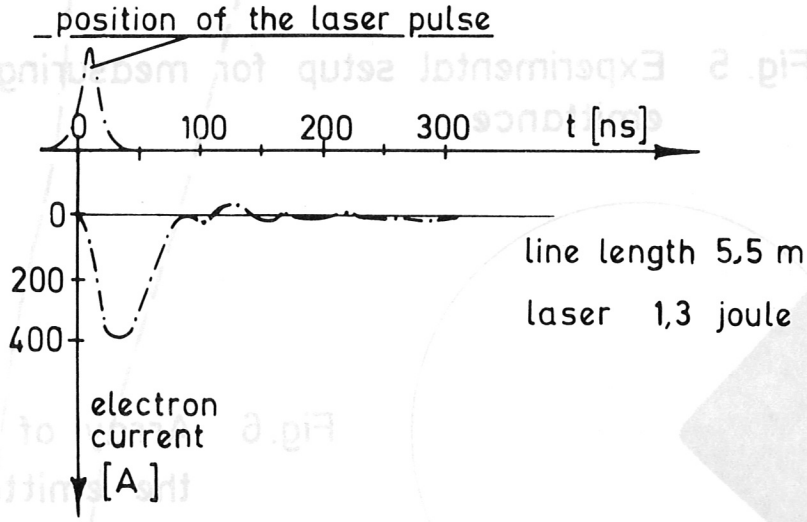

Fig. 3. Electron pulse

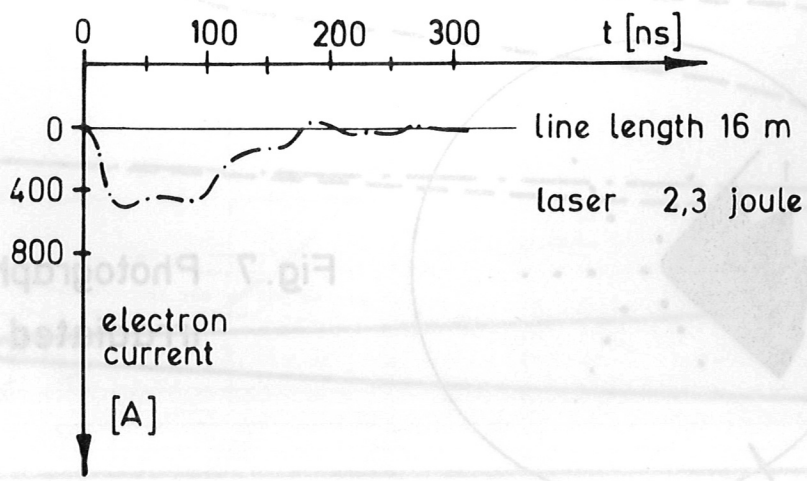

Fig 4. Electron pulse

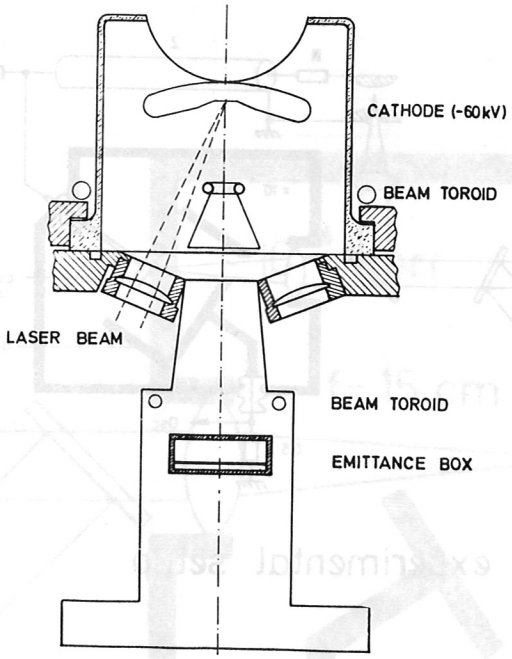

Fig. 5 Experimental setup for measuring the emittance

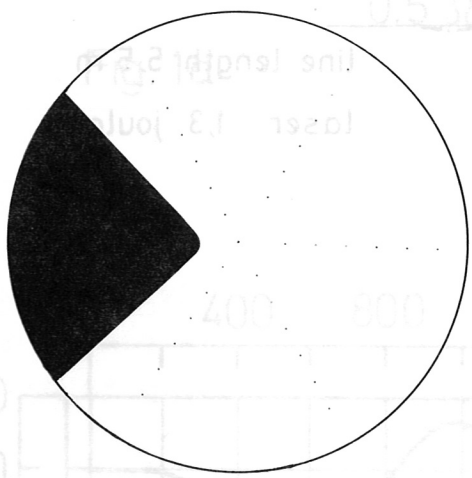

Fig. 6 Array of the holes in the emittance box

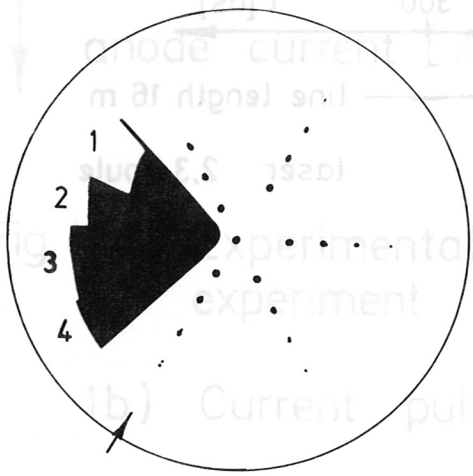

Fig. 7 Photograph of the irradiated film

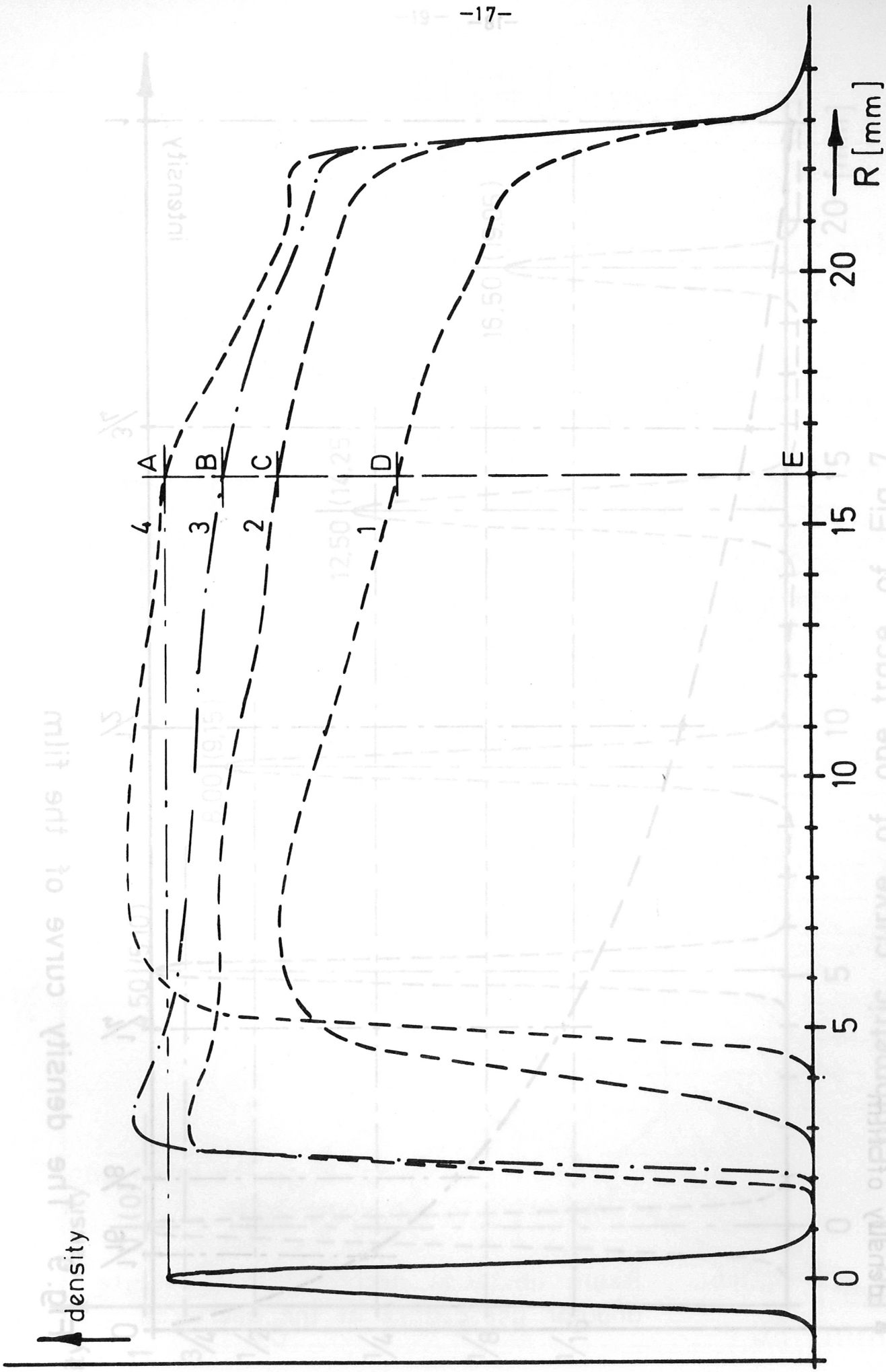

Fig. 8 Calibration of the film density

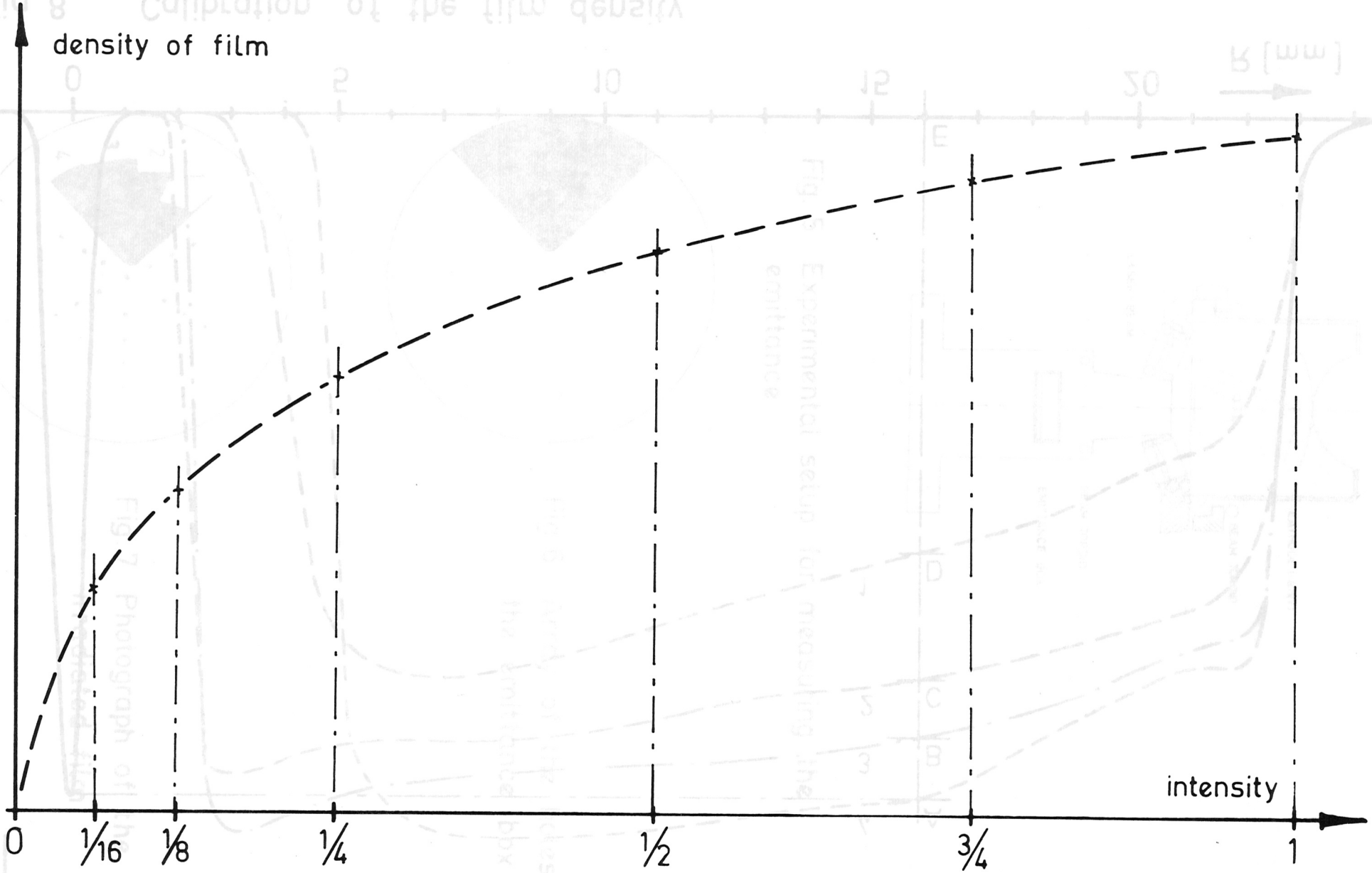

Fig. 9 The density curve of the film

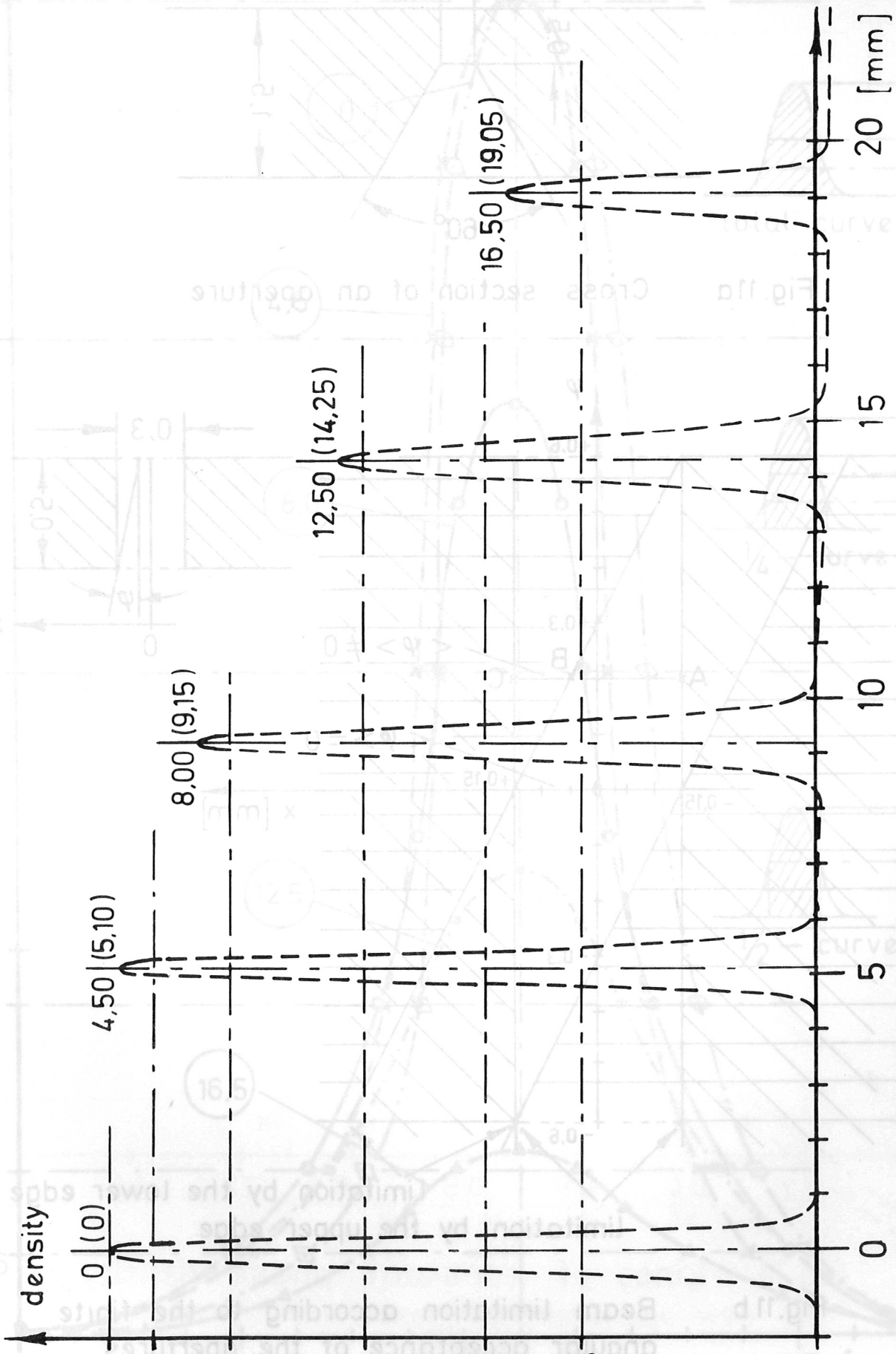

Fig. 10 Photometric curve of one trace of Fig. 7

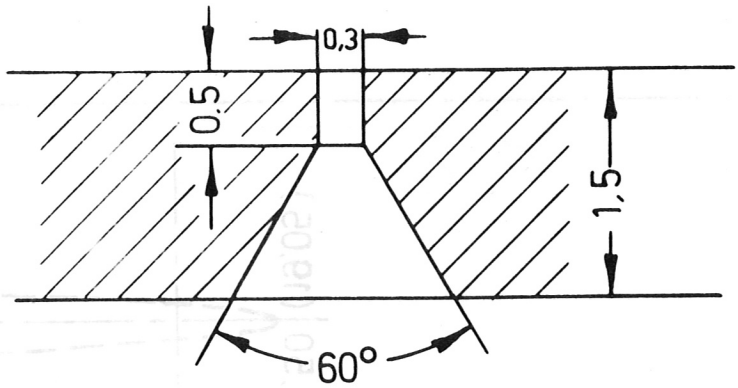

Fig. 11a Cross section of an aperture

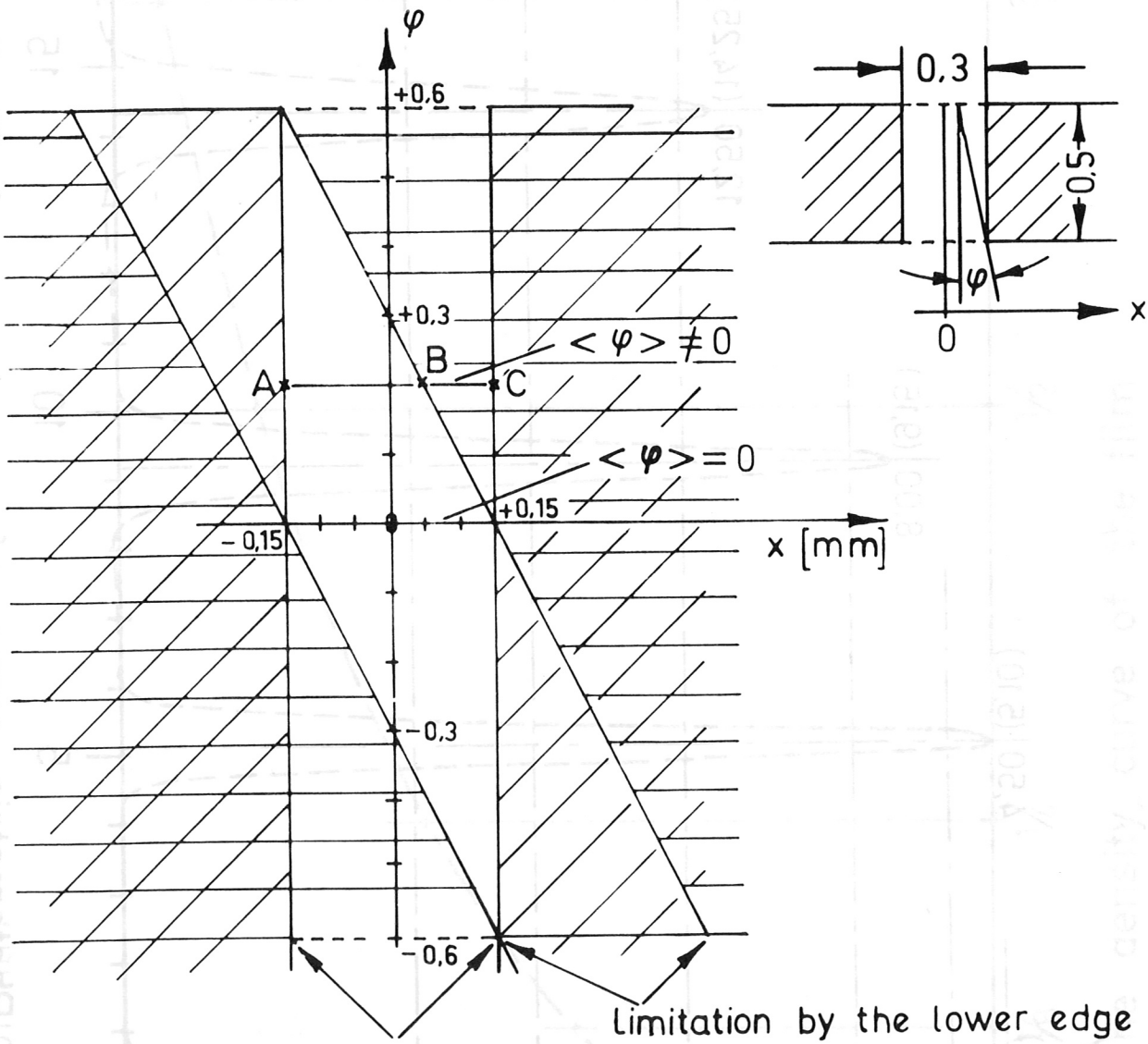

Fig. 11 b Beam limitation according to the finite angular acceptance of the apertures

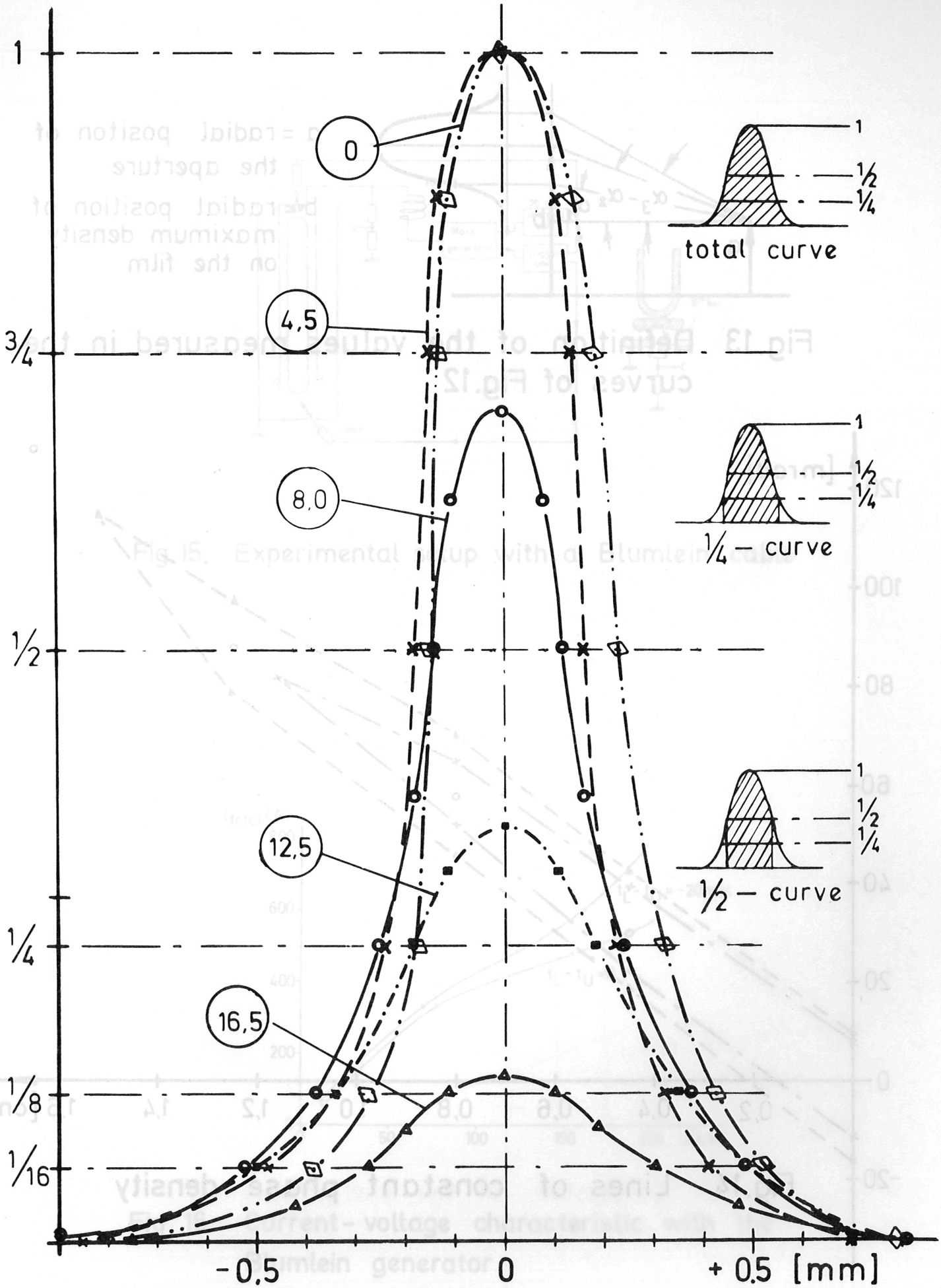

Fig. 12 Corrected photometric curves

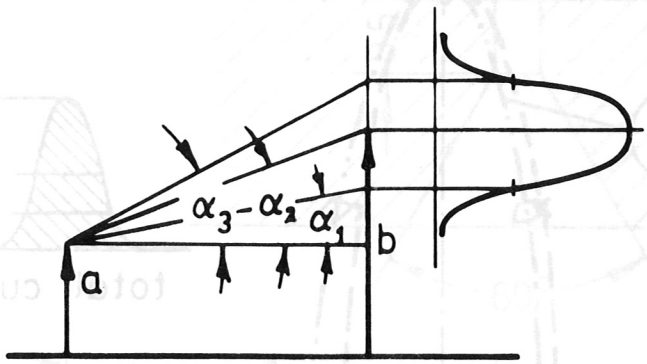

a = radial positon of the aperture

b = radial position of maximum density on the film

Fig.13 Definition of the values measured in the curves of Fig.12

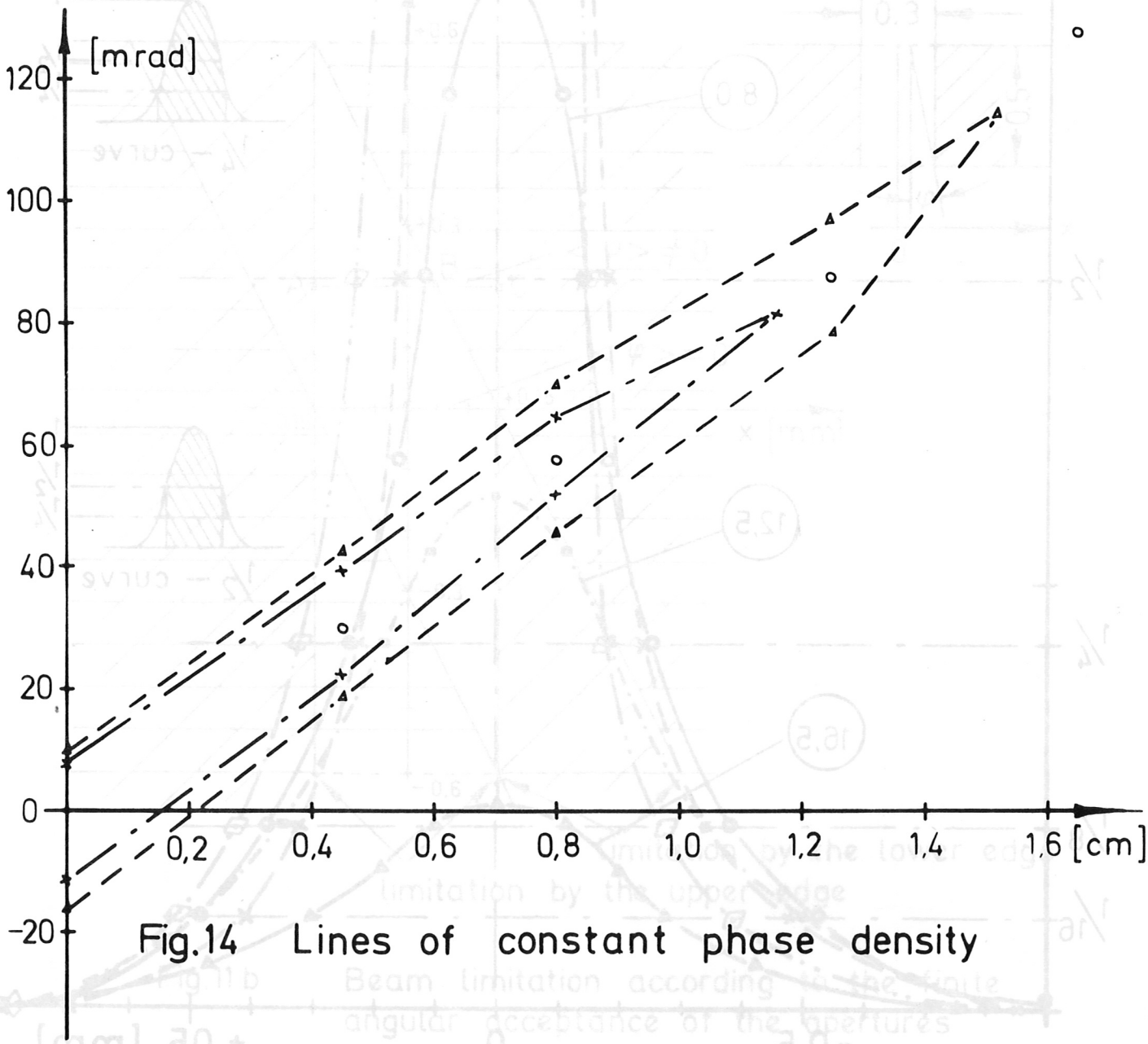

Fig.14 Lines of constant phase density

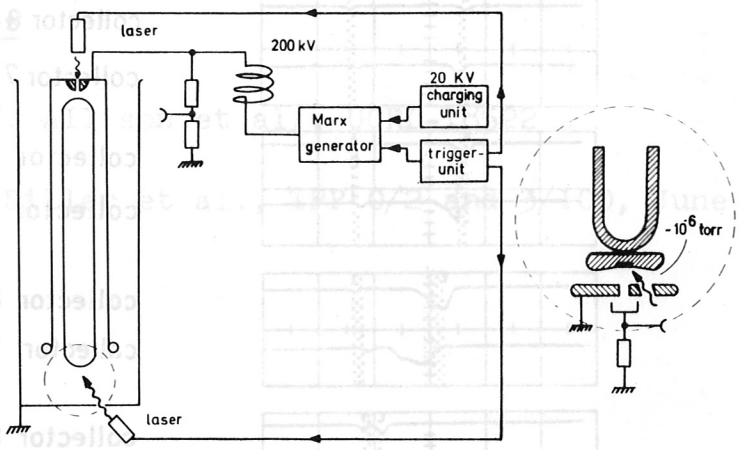

Fig.15. Experimental setup with a Blumlein cable

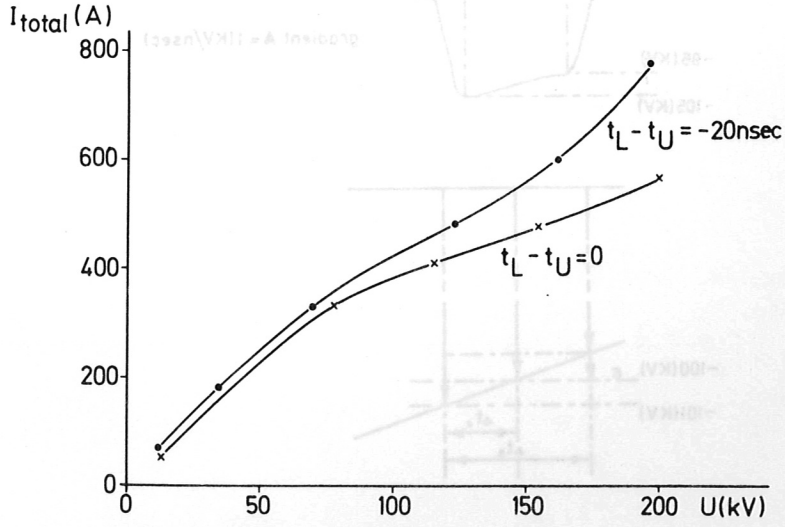

Fig. 16 Current - voltage characteristic with the Blumlein generator

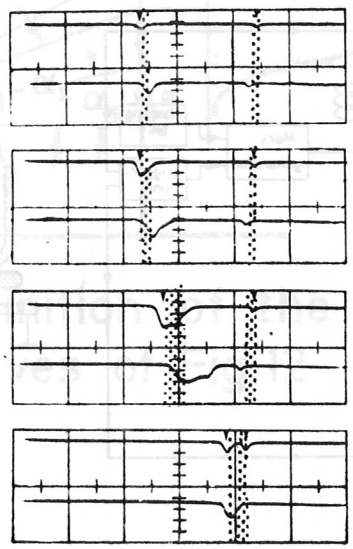

Fig. 17 Electron pulses in the magnetic spectrometer (5 nsec / div.)

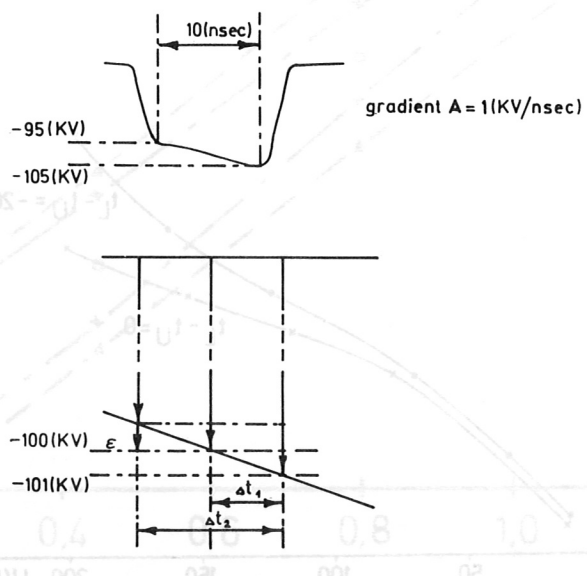

Fig. 18 Evaluation of the energy spread

References

1) R.W. Allison et. al., UCRL-18522

2) G. Siller et. al., IPP 0/2 and 3/100, June 1969